INTERNATIONAL JOURNAL OF PRECISION ENGINEERING AND MANUFACTURING Vol. 17, No. 11, pp. 1451-1463 NOVEMBER 2016 / 1451
DOI: 10.1007/s12541-016-0171-0 ISSN 2234-7593 (Print) / ISSN 2005-4602 (Online)

Adaptive Semi-Parallel Position/Force-Sensorless Control of Electro-Hydraulic Actuator System using MR Fluid Damper

Dao Thanh Liem[1] and Kyoung Kwan Ahn[2,#]

1 School of Mechanical Engineering, Graduate School, University of Ulsan, 93, Daehak-ro, Nam-gu, Ulsan, 44610, South Korea
2 School of Mechanical Engineering, University of Ulsan, 93, Daehak-ro, Nam-gu, Ulsan, 44610, South Korea
Corresponding Author / E-mail: kkahn@ulsan.ac.kr, TEL: +82-52-259-2282, FAX: +82-52-259-1680

KEYWORDS: Semi-parallel control, Electro-hydraulics actuator, MR fluid damper, Force-sensorless, Grey-markov predictor

The focus of this paper is to develop a semi-parallel control method using an inversion of identification model of a magneto-rheological (MR) fluid damper along with a smart predictor controller (SPC) for a damping system using that damper and an electro-hydraulic actuator (EHA) in order to realize the real time position/force control of the industrial task requiring interaction with the environment. The inverse model of MR fluid damper is established base on a self-tuning Lyapunov-based fuzzy (STLF) model. This STLF model is designed in the form of a center average fuzzy interference system, of which the fuzzy rules are planted based on the Lyapunov stability condition. In addition, in order to optimize the STLF model, the back propagation learning rules are used to adjust the fuzzy weighting net. Meanwhile, the SPC is constructed using a nonlinear PID controller (NPID) base on feedforward neural network and a smart Grey-Markov predictor (SGMP). Here, the NPID controller is built to drive the system to desired targets. Additionally, a learning mechanism with robust checking conditions is implemented into the NPID in order to optimize online its parameters with respect to the control error minimization. Besides, the SGMP with self-tuning ability of the predictor step size takes part in, first, estimating the system.

Manuscript received: May 16, 2016 / Revised: June 27, 2016 / Accepted: July 12, 2016

NOMENCLATURE

$u(t)$ = control signal
$u_{NPID}(t)$ = nonlinear PID output
G_{PID} = PID transfer function
$L(s)$ = open-loop transfer function
$S(s)$ = sensitivity function
M = gain margin
M_D = upper bound of the sensitivity
Y_g = sigmoid function's shape factor
$E(t)$ = error
η_p, η_i, η_d = learning rates
$\hat{y}(t+p)$ = system response in a near future
$y^{(0)}$ = output data point
$z^{(1)}$ = consecutive neighbor generation
p = Grey predictor step size
$P_{ij}^{(k)}$ = transition probability

1. Introduction

In the last decade, EHAs have shown significant advantages in industrial robot applications where force or position control with high accuracy is exceedingly necessary. In most cases, position control is appropriate when the industrial robot application is not requiring a compliant system to solve, but when any contact is made between the industrial robot end-effector and the environment, such as grinding, polishing, deburring, assembly and so on, position control might not suffice. It is necessary to control not only the position of the robot but also the contact force between the end-effector and the environment.[1] In these kinds of applications, the ability of force control systems to track varying desired signal is often required for the proper operation of the technological process. In addition, the task of position control of the hydraulic actuator is very important. Therefore, a new quality and significant improvement in the functioning of the press can be obtained with a simultaneous realization of position feedback, which is actually a hybrid control algorithm. Besides the benefits, in contrast to the

simplicity of EHAs, their control problem is very complicated due to nonlinearities and large uncertainties. Furthermore, working environments always contain unknown perturbations and disturbances that affect the control performances, such as stability, frequency response, or loading sensitivity. These problems cause many challenges for the modeling and design of feedback controllers for EHA applications. Numerous experimental systems using EHAs have been then conducted for doing research on how to improve the system performances.[2-6] Additionally, in order to overcome the control problems for these complex systems, several control strategies have been proposed.[7-10] In addition, the force control of hydraulics system for contacting tasks have been developed and discussed in Ref. 11. The comparison results by mean of real-time experiments proved convincingly that the proposed controller can enhance the acceptable performances. However, the force control strategies are to use force sensors where the reliability and accuracy are limited since the work-sites are filled with noise and thermal disturbances. Therefore, the demand for sensorless control is necessary considering sensors' cost and reliability in real time control strategies.

In force damping control problems, MR fluid damper which is capable of generating a force with magnitude sufficient for rapid response in large-scale applications has recently received more attention because they offer the adaptability of active control devices without requiring the associated large power sources,[12-17] while requiring only a battery for power.[17] Additionally, these devices offer highly reliable operations and their performance is relatively insensitive to temperature fluctuations or impurities in the fluid.[18] However, a major drawback that hinders its application rests with the nonlinear force-displacement and hysteretic force-velocity characteristics. Therefore, one of the challenges involved in creating high performance MR fluid damper in force damping control applications is the development of accurate models that can take full advantage of the unique features of the MR device. Both parametric and nonparametric models have been built by researchers to describe the behavior of MR fluid dampers.[19-25] However, these techniques demanded high computational cost to generate and optimize the model parameters and/or the model architectures and the training methods were complex.[26]

Base on the above analyses, a position/force damping test rig for the EHA using MR fluid damper named the electro-hydraulics damping system (EHDS) is developed in this paper in order to investigate the simultaneous position and force control performances. In this system, the EHA is used to support the position of the loading system as a guiding motion part while the MR fluid damper is used to support force as punch tool. Furthermore, for the purpose of improving force and position control performance with high precision of hybrid hydraulic systems, a semi-parallel position/force-sensorless control strategy is proposed in this paper for application of EHDS. The proposed control method is a combination of the smart predictive control (SPC), and MR fluid damper identification techniques using a self-tuning Lyapunov-based fuzzy approach (STLF). Here, the SPC is constructed using a nonlinear PID (NPID) and a smart Grey-Markov predictor (SGMP), which is developed from the typical single variable first order grey model GM (1,1) and Markov chain forecasting technique. First, the NPID is to drive the system to follow desired targets. To improve the control quality, the parameters of PID controller are online optimized

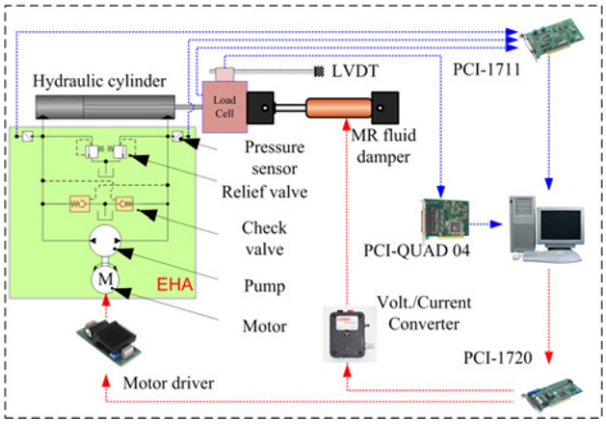

Fig. 1 Structure of experiment EHDS

with respect to the control error minimization by using a neural network-based learning mechanism under robust checking conditions which are theoretically designed to ensure the robust stability and disturbance rejection capability. Second, the SGMP bases on only a few historical system data to enhance two tasks: to estimate the system output in advance which is then used for deriving the control input and optimizing the control parameters; to compensate effectively the influences noises and disturbances on the system. Besides, the prediction step size, p, is online regulated by fuzzy inferences to reduce the settle time and overshoot problems of the control response. As a result, the overall control performance is significantly improved. Meanwhile, to obtain force-sensorless control ability, an inversion model of the MR fluid damper is implemented based on a developed STLFM model.[26] The STLFM model is constructed in form of a center average fuzzy inferences system, of which the fuzzy rules are designed based on the Lyapunov stability condition to estimate directly the MR damping force output which respect to the MR characteristics. In addition, the back propagation learning rules are used to adjust the fuzzy weighting net to optimize the STLFM model. In order to verify ability of a controller applied to the EHDS as in real working conditions, the electrical noise is also added to the feedback sensor signals of the control system. Experiments are carried out to show the high accuracy of both force and position control of the EHDS using the proposed semi-parallel control strategy, even in the varying external disturbance of the working environment.

2. Experimental set up of EHDS

To develop the suggested parallel control strategy as well as to investigate its applicability, an experimental system using a commercial EHA and MR fluid damper has been set up. The system configuration is depicted in Fig. 1. In this system, an EHA (Bosch Rexroth C1620S153) which includes a gear pump, a supplementary valves system driven by a proper driver was installed to adjust the movement of the main cylinder (D × d × L = 35 × 14 × 500 mm). The speed of the motor is driven by a Devantech MD03 DC motor driver. To generate the load for the system, a MR fluid damper (Lord RD-1005-3) was then attached to the end-effector of the hydraulic cylinder. In the

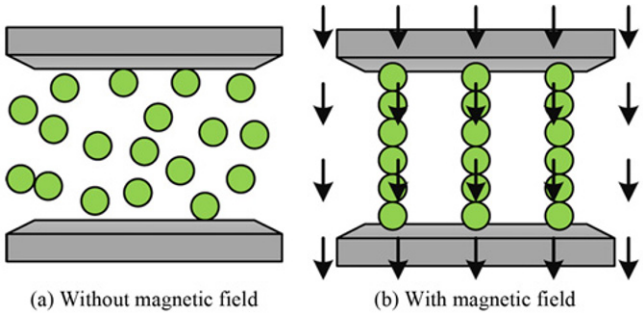

Fig. 2 The working principle of MR fluid

presence of an applied current (as well as magnetic field inside the MR fluid damper), the iron particles acquire a dipole moment aligned with the external field which causes particles to form linear chains parallel to the field, as described in Fig. 2. This phenomenon can solidify the suspended iron particles and restrict the fluid movement. Consequently, yield strength is developed within the fluid. The degree of change is related to the magnitude of the applied magnetic field, and can occur only in a few milliseconds. By employing the MR damper with ability to change its viscosity corresponding to the applied current through a voltage/current converter (Rheonetic Wonder Kit), any desired loading profile could be achieved. A linear variable differential transformer (LVDT WTB 5-0500MM) was employed to measure the piston-rod displacement of the cylinder (which is sent to the SPC control to perform the position control part) while a compatible load cell with 2000N capacity made by Bongshin Corp. was attached in series with the cylinder rod to measure the loading force (which is used to compared with the force estimated by the STLFM model as well as to investigate the force-sensorless control performance).

For the control part, a compatible PC a 12-bit A/D PCI board (Advantech, PCI 1711 card), a D/A PCI board (Advantech, PCI 1720 card) and a 32-bit Computing Measurement counter board, PCI Quad-04, were used to convert in turn the LVDT and load cell signals to position and force data which are used for the further investigations, and developments of the control system. Here, a software control algorithm for the system was coded in C-mex programming language combined with Real-Time Windows Target of Matlab/Simulink environment with 0.01s of sampling period to perform the control verification. Finially, the experimental apparatus is set up and displayed in Fig. 3.

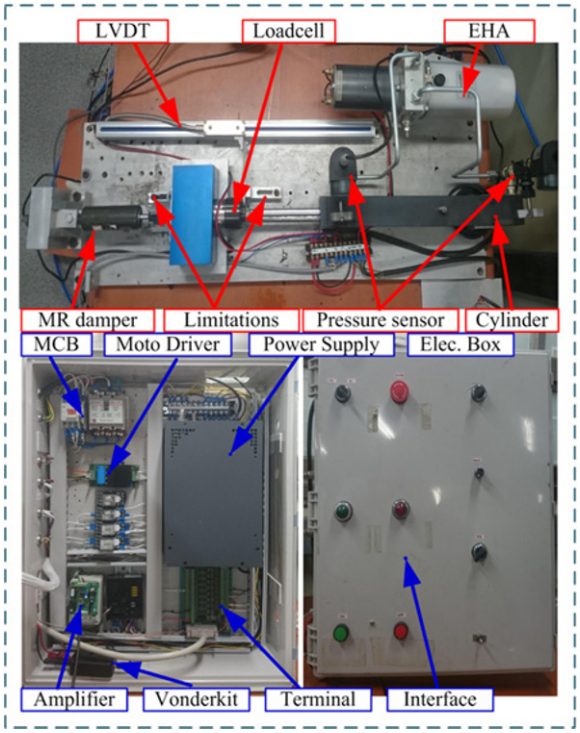

Fig. 3 Experimental set up of EHDS

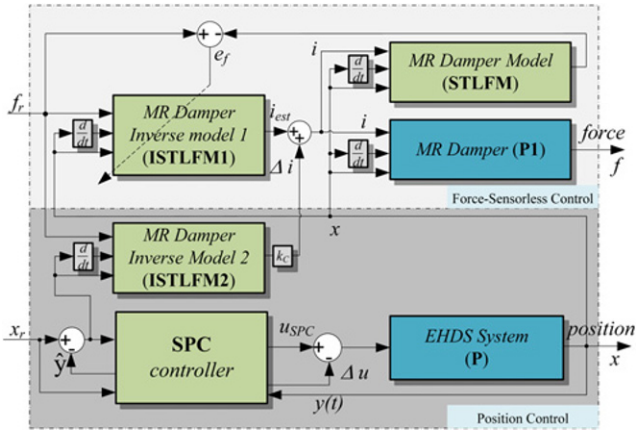

Fig. 4 Structure of semi-parallel position/Force-sensorless damping control system

3. Semi-Parallel Position and Force-Sensorless Controller Design

As introduced above, the proposed semi-parallel control method is presented in Fig. 4. Here, the controller consists of two main parts which respect to the force and position generators. First the two position and force-sensorless controllers are used to compute the control signal i_{est} and u_{SPC} that are sent to the position and force generator by using the SPC and ISTLFM1, respectively. Furthermore, the predicted displacement error obtained by the SPC is then used to estimate the additive compensated control signal, *Di*, using ISTLFM2 which is added to the applied current to improve the control performance. Finally, the control signal *i* for the force generator, which is ensure the force control performance, is increase with an amount equal to the additional control signal, D*i*, to compensate the position and force-sensorless control performance with the position generator. As a result, the design control algorithm has enough control ability for the application for the EHDS with the desirable position and force performance.

3.1 Design of force-sensorless control system

As described in Introduction, the force-sensorless control system is implemented base on the developed STLFM model. The designed

STLFM model contains two parts: one is the Lyapunov-fuzzy inference (LFI) to estimate the damping force caused by the displacement of the damper rod, and the other is the gain fuzzy inference (GFI) to switch between the damping force levels with respect to the current supplied for the damper coil. In this STLFM model, the stability condition by using Lyapunov are determined to design the fuzzy inference and guarantee the relationship between the model input (piston displacement and velocity) and the output (estimated damping force). By analyzing the relation between the MR damper displacement, velocity, acceleration and damping force, as one experiment shown in Fig. 5, it can be seen that the MR damping behavior which respect to a fixed supply current could satisfy the sufficient robust condition.

$$\dot{V}<0 \Leftrightarrow \begin{bmatrix} x,\dot{x}>0,\ddot{x}<-x; \\ x,\dot{x}<0,\ddot{x}>-x; \\ x>0,\dot{x}<0,\ddot{x}>-x; \\ x<0,\dot{x}>0,\ddot{x}<-x; \end{bmatrix} \tag{1}$$

where, $V(x)$ is the Lyapunov function candidate, x is the input of the system. The fuzzy rules are finally established based on the damping behavior to hold the condition (1). Besides, a damping system using this damper was also setup to investigate the design model and experimental was carried out to evaluate the effectiveness of the STLFM model.

Based on the advantages of the direct modeling method for the MR damper using the STLFM model, the inverse model, ISTLFM1, has been derived as the damping force controller. The optimized STLFM has been used to set initial parameters for the ISTLFM1. The ISTLFM1 model estimates current levels should be applied to the damper to create desired damping forces. The key idea in this proposed control method is to control the damping force without using any force sensor. As a result, the optimized STLFM model is combined in the control system as a virtual force sensor to predict the actual damping force. This predicted force with the desired force are fed back to the ISTLFM1 controller to generate the control signal to MR fluid damper and, hence, to perform closed-loop damping control.

Consequently, the force-sensorless control system is described as in Fig. 6. From this figure, the ISTLFM1 model contains two parts. The first part is a Lyapunov-based fuzzy inference (LFI'), which was derived from LFI system of the optimized STLFM model, to estimate the damping force (u) of the MR fluid damper. The second part is an inverse gain fuzzy inference (IGFI) which was developed from GFI system of the optimized STLFM model. The IGFI provides the current (I_{MR_est}) level needed to supply for the MR damper to generate the damping force level (k). This damping force level can be computed from the damping force (f_{MR_est}) estimated by using the STLFM and the estimated damping force (u) caused by the damper rod displacement/velocity.

$$k = \begin{cases} f_{MR\_est} / u & if\ u \neq 0 \\ 0 & if\ u = 0 \end{cases} \tag{2}$$

For improving the ISTLFM1 control accuracy, an error function (E') was derived from the difference between the damping force (f_{MR_est}) measured by the STLFM and the desired force (f_{MR_ref}) as

$$E' = 0.5(f_{MR\_est} - f_{MR\_ref})^2 \tag{3}$$

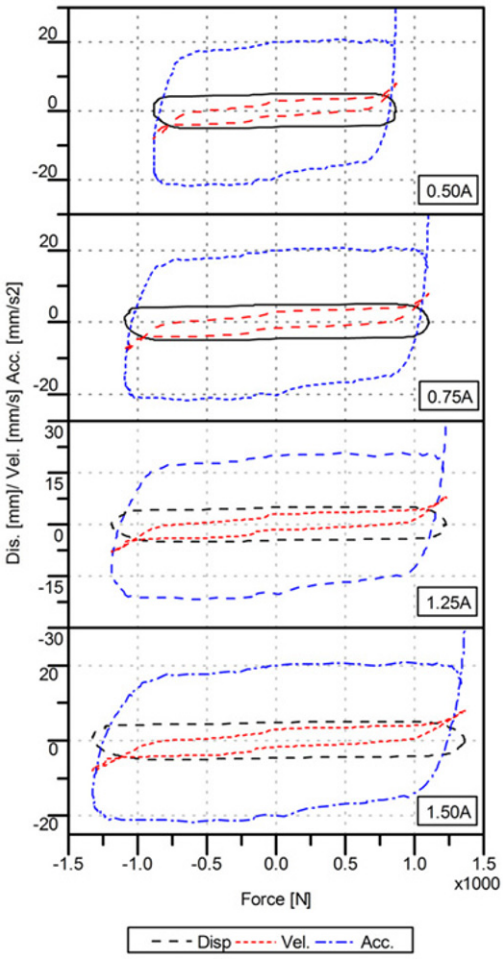

Fig. 5 Experimental investigation: displacement, velocity and acceleration vs. force at a sinusoidal exc. (2.5 Hz and 5 mm)

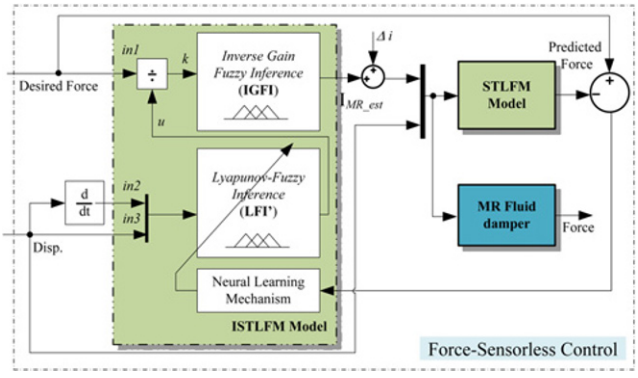

Fig. 6 General view of force-sensorless control system design

$$\left.\begin{aligned} a_{ji}\big|_{t+1} &= a_{ji}\big|_t - \eta'_a \frac{\partial E'}{\partial a_{ji}}\Big|_t \\ b_{ji}\big|_{t+1} &= b_{ji}\big|_t - \eta'_b \frac{\partial E'}{\partial b_{ji}}\Big|_t \\ w_k\big|_{t+1} &= w_k\big|_t - \eta'_w \frac{\partial E'}{\partial w_k}\Big|_t \end{aligned}\right\} \tag{4}$$

where η'_a, η'_b and η'_w are the learning rates. The factor $\partial E'/\partial w_k$ in Eq. (4) can be calculated as

$$\frac{\partial E'}{\partial w_k} = \frac{\partial E'}{\partial f_{MR\_est}} \frac{\partial f_{MR\_est}}{\partial I_{MR\_est}} \frac{\partial I_{MR\_est}}{\partial k} \frac{\partial k}{\partial u} \frac{\partial u}{\partial w_k} \tag{5}$$

where:

$$\frac{\partial E'}{\partial f_{MR\_est}} = e'(t) = f_{MR\_est}(t) - f_{MR\_ref}(t) \tag{6}$$

$$\frac{\partial f_{MR\_est}}{\partial I_{MR\_est}} \approx \left. \frac{\delta f_{MR\_est}}{\delta I_{MR\_est}} \right|_t \tag{7}$$

$$\frac{\partial I_{MR\_est}}{\partial k} \approx \left. \frac{\delta I_{MR\_est}}{\delta k} \right|_t \tag{8}$$

$$\frac{\partial k(t)}{\partial u(t)} = -\frac{f_{MR\_est}}{u^2} \tag{9}$$

$$\frac{\partial u}{\partial w_k} = \frac{\mu(w_k)}{\left(\sum_{l=1}^{M} \mu(w_l)\right)} \tag{10}$$

The next factors $\partial E'/\partial a_{ji}$ in Eq. (4) can be computed by:

$\frac{\partial E'}{\partial a_{ji}} = \frac{\partial E'}{\partial u} \frac{\partial u}{\partial \mu_j(x_i)} \frac{\partial \mu_j(x_i)}{\partial a_{ji}}$, where: $\partial E'/\partial u$ is calculated by using Eqs. (6)~(9).

$$\frac{\partial u}{\partial \mu_j(x_i)} = \frac{\partial u}{\partial \mu(w_k)} = \frac{\sum_{l=1}^{M} \mu(w_l)(w_k - w_l)}{\left(\sum_{l=1}^{M} \mu(w_l)\right)^2} \tag{11}$$

$$\frac{\partial \mu_j(x_i)}{\partial a_{ji}} = sign(x_i - a_{ji}) \frac{2}{b_{ji}} \tag{12}$$

The final factor $\partial E'/\partial b_{ji}$ in Eq. (4) can be found by:

$$\frac{\partial E'}{\partial b_{ji}} = \frac{\partial E'}{\partial u} \frac{\partial u}{\partial \mu_j(x_i)} \frac{\partial \mu_j(x_i)}{\partial b_{ji}} \tag{13}$$

where: $\partial E'/\partial u$ and $\partial u/\partial \mu_j(x_i)$ are calculated by using Eqs. (10)-(13), and (14), respectively.

$$\frac{\partial \mu_j(x_i)}{\partial b_{ji}} = \frac{2|x_i - a_{ji}|}{{b_{ji}}^2} \tag{14}$$

By using the above self-learning algorithm (Eqs. (4)-(14)), the LFI' can work more precisely in estimating the damping force (u) with respect to the displacement/velocity.

Additionally, another inverse model, ISTLFM2, is constructed with the same principle of ISTLFM1 to estimate the additive control signal of the MR fluid damper based on the predicted displacement error information given by the SPC controller. This additive signal is then sent to the force control system to balance the position and force control performance through a conversion gain k_c.

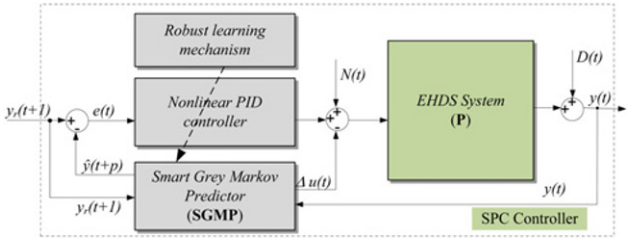

Fig. 7 General structure of SPC controller

$$i = i_{est} + \Delta i \tag{15}$$

3.2 Design of smart predictive controller (SPC)

As described in the Introduction, the SPC is constructed using a nonlinear PID controller based on feedforward neural network and a SGMP as shown in Fig. 7.

Here, the NPID controller is built to drive the system to desired targets. Additionally, a learning mechanism with robust checking conditions is implemented into the NPID in order to optimize online its parameters with respect to the control error minimization. Meanwhile, the SGMP with self-tuning ability of the predictor step size takes part in, first, estimating the system output in the near future to optimize the controller parameters in advance and, second, creating a compensating control signal accordingly to the system perturbations and, consequently, improving the control performance.

3.3 Nonlinear PID controller design

As mentioned before, the NPID controller consists of the neural network-based PID control block and robust learning mechanism. According to the control error, $e(t)$, the proper driving command, $u_{NPID}(t)$, is produced using the NPID algorithm. Synchronously, the PID gains, K_p, K_i, and K_d, are tuned by the robust learning mechanism which is based on back propagation method and robust constrains. Since, the superb mixture of conventional PID controller and neural network has the powerful capability of learning, adaptation and tackling nonlinearity and, consequently, provides a good tracking performance. The procedure to design this control module is as the followings.

First, the control problem is taken into account in a single input and single output system. The main control signal of the system can be obtained in the time domain as bellow:

$$u_{NPID}(t) = u(t-1) + u_{NN}(t) \tag{16}$$

where: $u_{NPID}(t)$ and $u(t-1)$ are in turn control signal in t and $(t-1)$; $u_{NN}(t)$ is the output of the feedforward neural network structure. The $u_{NN}(t)$ can be described as follows:

$$u_{NN}(t) = f(x(t)) = \frac{2\left(1 - e^{-x.Y_g}\right)}{Y_g\left(1 + e^{-x.Y_g}\right)} \tag{17}$$

where, Y_g is the parameter which determines the shape of the sigmoid function; x is the input of the sigmoid function which is computed using the PID algorithm:

$$x(t) = u_{PID}(t) = K_p(t)e_p(t) + K_i(t)e_i(t) + K_d(t)e_d(t) \quad (18)$$

where, $e_p(t)$ is the error between the desired set point and the estimated system output; $e_d(t)$ is the derivation of error $e(t)$; $e_i(t)$ is the integral of error $e(t)$; $u_{PID}(t)$ is the PID control signal; K_p, K_i, and K_d are the proportional gain, integral gain, and derivative gain, respectively.

Second, these PID gains, K_p, K_i, and K_d are tuned using back propagation learning algorithm as:

$$\begin{cases} K_p(t+1) = K_p(t) - \eta_p \dfrac{\partial E(t)}{\partial K_p} \\ K_i(t+1) = K_i(t) - \eta_i \dfrac{\partial E(t)}{\partial K_i} \\ K_d(t+1) = K_i(t) - \eta_d \dfrac{\partial E(t)}{\partial K_i} \end{cases} \quad (19)$$

where η_p, η_i, and η_d are the learning rates determining the convergence speeds of updated control gains; $E(t)$ is an error function which is defined as

$$E(t) = \frac{1}{2}\left(y_{ref}(t) - \hat{y}(t)\right)^2 \quad (20)$$

where, $y_{ref}(t)$ and $\hat{y}(t+p)$ are the desired set point output and the estimated output, respectively.

From Eqs. (17), (19) and (20), it leads to the following equation:

$$\begin{cases} K_p(t+1) = K_p(t) + \eta_p e_p^2(t)\Delta \dfrac{4e^{-x.Y_g}}{\left(1+e^{-x.Y_g}\right)^2} \\ K_i(t+1) = K_i(t) + \eta_i e_p(t) e_i(t)\Delta \dfrac{4e^{-x.Y_g}}{\left(1+e^{-x.Y_g}\right)^2} \\ K_d(t+1) = K_i(t) + \eta_d e_p(t) e_d(t)\Delta \dfrac{4e^{-x.Y_g}}{\left(1+e^{-x.Y_g}\right)^2} \end{cases} \quad (21)$$

Third, in order to stabilize the control system, the robust updating rule is implemented into the learning mechanism to refine the PID gains. For robust control approach, there are two control objectives: closed-loop robust stability which must be checked with reasonable margins; and closed-loop disturbance attenuation.[27] From Eq. (18), the transfer functions of the PID controller, system open-loop and sensitivity function are expressed as followings:

$$G_{PID} = K_p + K_i\frac{1}{s} + K_d s \quad (22)$$

$$L(s) = P(s)G_{PID}(s) \quad (23)$$

$$S(s) = \frac{1}{1+L(s)} \quad (24)$$

For the robust stability, an approximately minimal value of $M = 1.4$ (3 dB) gain margin for the closed-loop system is given by:

$$\left|\frac{L(s)}{1+L(s)}\right| \le M = 1.4 \quad (25)$$

For the disturbance rejection requirement, the general upper bound of the sensitivity is set to limit the peak value of disturbance amplification as

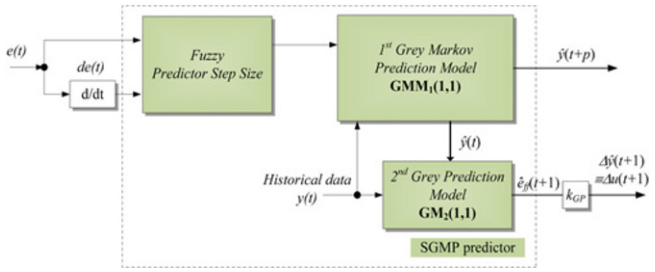

Fig. 8 The structure of SGMP model

$$\left|\frac{L(s)}{1+L(s)}\right| \le M_D, \quad M_D > 1 \quad (26)$$

Finally, for each working step, the PID control gains are robustly updated to satisfy the robustness requirements as the following rule:

$$K_a(t+1) = \begin{cases} K_a(t+1) \text{ using (18) if: satisfy (25) \& (26)} \\ K_a(t) \qquad \text{otherwise} \end{cases} \quad (27)$$

(a is p,i or d)

3.4 SGMP predictor design

In the most ideal situation, feedforward control can totally eliminate the effect of the measured disturbance on the system. However, the use of feedforward control depends on whether the degree of improvement in response to the measured disturbance justifies the added costs of implementation and maintenance.[28] Besides, this use leads to many requirements such as a mathematical model of the system, knowing control signal and/or effect of the system output to the load.[29] To overcome these weaknesses, grey predictor is a proper tool to provide knowledge of the system process and disturbances as well.[30-35] Since the control of EHDS system is affected by variant random factors, highly complex nonlinearities and large uncertainties in the systems, etc., the prediction performance could not be always enhanced by single grey model.[36-38] The more the characteristics that relate to the system dynamics are considered, the better prediction performance could be achieved. Therefore, Markov chain forecasting method[39-41] combined with the *GM* (1,1) is then developed to further achieve the predicted accuracy.

In grey prediction theory, *GM* (*n, m*) denotes a grey model, where *n, m* are the order of the difference equation and the number of variables. *GM* (1,1), the most popular grey model, is then used to develop the SGMP of which the structure is shown in Fig. 8. As seen in this figure, the FGP contains two inputs – the historical data of desired output, $y_r(t)$, and actual response, $y(t)$, and two outputs, $\hat{y}(t+p)$ and $Du(t)$. Based on the observation of system responses, the first Grey-Markov model, GMM_1 (1,1), with dynamic FPSS estimates the system response in the near future, $\hat{y}(t+p)$, which is sent to the main control unit to perform the control signal. At the same time, the GMM_1 (1,1) also carries out the predicted system response at present which is sent to the second grey model, GM_2 (1,1), to estimate the effect of noises and disturbances on the system response and, consequently, to produce the correspondingly compensating control signal, $Du(t)$. The two outputs are then sent to the proposed control scheme to perform the

closed-control loop (see Fig. 7).

3.4.1 The first Grey-Markov prediction model GMM_1 (1,1)

As presented in Ref. 28, the grey prediction procedure of *GM* (1,1) model is as follows:

Step 1: At least four output data points are needed to approximate a system. For a nonnegative time series, n raw data is collected as:

$$y^{(0)}=\left\{y^{(0)}(t-n+1),y^{(0)}(t-n+2),...,y^{(0)}(t)\right\};\ n\geq 4 \tag{28}$$

Step 2: Use the accumulated generating operation (AGO) to obtain $y^{(1)}$ from $y^{(0)}$

$$y^{(1)}(t_k)=\sum_{i=1}^{t_k}y^{(0)}(i)\quad t_k=t-n+1,t-n+2,...,t \tag{29}$$

Step 3: Apply a consecutive neighbor generation $z^{(1)}$ from $y^{(1)}$ by the following mean generating operation (MGO):

$$z^{(1)}(t_k)=\frac{1}{2}\left(y^{(1)}(t_k)+y^{(1)}(t_k-1)\right) \tag{30}$$

Step 4: Establish grey differential equation of *GM* (1,1):

$$y^{(0)}(t_k)+az^{(1)}(t_k)=b \tag{31}$$

In which, parameter [*a*, *b*] can be obtained by using the least square method as follows:

$$\hat{a}=\begin{bmatrix}a\\b\end{bmatrix}=\left(B^TB\right)^{-1}B^TY \tag{32}$$

Where

$$B=\begin{bmatrix}-z^{(1)}(2) & 1\\ -z^{(1)}(3) & 1\\ \vdots & \vdots\\ -z^{(1)}(t) & 1\end{bmatrix}\qquad Y=\begin{bmatrix}y^{(0)}(2)\\ y^{(0)}(3)\\ \vdots\\ y^{(0)}(t)\end{bmatrix} \tag{33}$$

Step 5: Set up the prediction model *GM* (1,1) as:

$$\hat{y}^{(1)}(t_k+1)=\left(y^{(1)}(1)-\frac{b}{a}\right)e^{-at_k}+\frac{b}{a} \tag{34}$$

$$\hat{y}^{(0)}(t_k+1)=y^{(1)}(t_k+1)-y^{(1)}(t_k) \tag{35}$$

Step 6: Calculate the predictive output at $(t+p)^{th}$ step, $\hat{y}^{(0)}(t+p)$: (p is the prediction step size)

$$\hat{y}^{(1)}(t+p)=\left(y^{(1)}(1)-\frac{b}{a}\right)e^{-a(t+p-1)}+\frac{b}{a} \tag{36}$$

$$\hat{y}^{(0)}(t+p)=y^{(1)}(t+p)-\hat{y}^{(1)}(t+p-1) \tag{37}$$

3.4.2 Partition of states by Markov chain forecasting model

As mentioned before, in the SGMP predictor, Markov chain combined with the *GM* (1,1) is developed to further achieve the predicted accuracy. The predicted output value $\hat{y}^{(0)}$ is obtained by *GM* (1,1) model causes the residual error $e(i)=y^{(0)}-\hat{y}^{(0)}$. Then the Markov state transition matrix can be established in which the states are defined for each time step. The residual errors are partitioned in to equal portions, each state interval whose width is equal to a fixed portion of the residual error. Finally, the actual error can be classified into those states. The Markov chain is determined as follows:

$$P\left(X_{n+k}=q_{n+k}\middle|X_n=q_n,...X_1=q_1\right)=P\left(X_{n+k}=q_{n+k}\middle|X_n=q_n\right) \tag{38}$$

where, q_n, q_n, …, q_n, …, q_{n+k} take discrete values in a state set $\eta_q=\{\Theta_1, \Theta_2, \ldots, \Theta_n\}$.

A *k*-step transition probability for the Markov chain of X_n with *N* states is represented as in Eq. (39):

$$P_{ij}(n,n+k)=P\left(q_{n+k}=\Theta_j\middle|q_n=\Theta_i\right)\quad 1\leq i,j\leq N \tag{39}$$

The transition probability of state is defined as:

$$P_{ij}^{(k)}=\frac{m_{ij}^{(k)}}{M_i} \tag{40}$$

In Eq. (40) $m_{ij}^{(k)}$ represents the number of state E_i transferred into state E_j by *k* steps and M_i introduces to number of appearances of state E_i. Then, the transition probability matrix of state can be written as:

$$P^{(k)}=\begin{bmatrix}p_{11}^{(k)} & p_{12}^{(k)} & \cdots & p_{1m}^{(k)}\\ p_{21}^{(k)} & p_{22}^{(k)} & \cdots & p_{2m}^{(k)}\\ \cdot & \cdot & \cdots & \cdot\\ \cdot & \cdot & \cdots & \cdot\\ \cdot & \cdot & \cdots & \cdot\\ p_{m1}^{(k)} & p_{m2}^{(k)} & \cdots & p_{mm}^{(k)}\end{bmatrix} \tag{41}$$

Since the future state transistion of system is determined, the determination of grey elements E_{1i} and E_{2i} the changing intervals of the estimation value is between E_{1i} and E_{2i}

where, $E_i=[E_{1i},E_{2i}]$, $\hat{E}_i\in E_i$, $i=(1, 2, \ldots, S)$ S is the amount of states and $\hat{E}_{1i}=\hat{y}^{(0)}(t+p)+A_i$, $\hat{E}_{2i}=\hat{y}^{(0)}(t+p)+B_i$.

The most probable predicted value of the system is obtained as:

$$\hat{y}(t+p)=\frac{1}{2}\left(E_{1i}+E_{2i}\right)=y(t+p-1)+\frac{1}{2}(A_i+B_i)\times\overline{Y} \tag{42}$$

where, $\overline{Y}$ is the average value of the historical data.

3.4.3 Improvement of designed prediction model

According to the complexity of the system, a forecasting model produces random error and bad data in every prediction. The relative error is considered as an indicator of prediction accuracy:

$$e(i)=\frac{y^{(0)}(i)-\hat{y}^{(0)}(i)}{y^{(0)}(i)},\ i=1,2,..,n \tag{43}$$

From Eq. (34) the prediction function can be obtained as:

$$\hat{y}^{(1)}(t_k+1)=\left(y^{(1)}(1)-\frac{b}{a}\right)e^{-at_k}+\frac{b}{a}=\Psi\ \times(1-e^a)^{-1}e^{-at_k}+\frac{b}{a} \tag{44}$$

$$\hat{y}^{(0)}(t_k+1)=\Psi\times e^{-at_k} \tag{45}$$

where, $\Psi_k=\left(y^{(1)}(1)-\frac{b}{a}\right)$, $\Psi=\Psi_k\times(1-e^a)$

Denote $Z(\Psi)=\sum_{i=1}^{n}\left(\frac{y^{(0)}(i)-\hat{y}^{(0)}(i)}{y^{(0)}(i)}\right)^2$, one has:

$$Z(\Psi)=\left(\frac{y^{(0)}(1)-\Psi_k-\frac{b}{a}}{y^{(0)}(1)}\right)^2+\sum_{i=2}^{n}\left(\frac{y^{(0)}(i)-\hat{y}^{(0)}(i)}{y^{(0)}(i)}\right)^2$$

$$=\left(\frac{y^{(0)}(1)-\Psi_k\times(1-e^{a})^{-1}-\frac{b}{a}}{y^{(0)}(1)}\right)^2+\sum_{i=2}^{n}\left(\frac{y^{(0)}(i)-\Psi_k\times(1-e^{a(i-1)})^{-1}}{y^{(0)}(i)}\right)^2$$

To minimize the relation error that is $dZ(\Psi)/d\Psi = 0$. It leads to the following equations:

$$\begin{aligned}\frac{dZ(\Psi)}{d\Psi}&=2\left(\frac{y^{(0)}(1)-\Psi_k\times(1-e^{a})^{-1}-\frac{b}{a}}{y^{(0)}(1)}\right)\times\frac{-(1-e^{a})^{-1}}{y^{(0)}(1)}\\&+\sum_{i=2}^{n}2\left(\frac{y^{(0)}(i)-\Psi_k\times(1-e^{a(i-1)})^{-1}}{y^{(0)}(i)}\right)\times\frac{-e^{a(i-1)}}{y^{(0)}(i)}\\&=2\Psi\times\left(\frac{(1-e^{a})^{-1}}{y^{(0)}(1)}\right)^2-2\frac{\left(y^{(0)}(1)-\frac{b}{a}\right)(1-e^{a})^{-1}}{y^{(0)}(1)}\\&+\sum_{i=2}^{n}2\left(\Psi\times\left(\frac{e^{-a(i-1)}}{y^{(0)}(i)}\right)^2-\frac{e^{-a(i-1)}}{y^{(0)}(i)}\right)=0\end{aligned}\tag{46}$$

Then, Ψ can be determined as bellows:

$$\Psi=\frac{\frac{\left(y^{(0)}(1)-\frac{b}{a}\right)(1-e^{a})^{-1}}{y^{(0)}(1)^2}+\sum_{i=2}^{n}\frac{e^{-a(i-1)}}{y^{(0)}(i)}}{\left(\frac{(1-e^{a})^{-1}}{y^{(0)}(1)}\right)^2+\sum_{i=2}^{n}\left(\frac{e^{-a(i-1)}}{y^{(0)}(i)}\right)^2}\tag{47}$$

Then the prediction function can be obtained as:

$$\hat{y}^{(1)}(t_k+1)=\frac{\frac{\left(y^{(0)}(1)-\frac{b}{a}\right)(1-e^{a})^{-1}}{y^{(0)}(1)^2}+\sum_{i=2}^{n}\frac{e^{-a(i-1)}}{y^{(0)}(i)}}{\left(\frac{(1-e^{a})^{-1}}{y^{(0)}(1)}\right)^2+\sum_{i=2}^{n}\left(\frac{e^{-a(i-1)}}{y^{(0)}(i)}\right)^2}(1-e^{a})^{-1}e^{-at_k}+\frac{b}{a}\tag{48}$$

$$\hat{y}^{(0)}(t_k+1)=\frac{\frac{\left(y^{(0)}(1)-\frac{b}{a}\right)(1-e^{a})^{-1}}{y^{(0)}(1)^2}+\sum_{i=2}^{n}\frac{e^{-a(i-1)}}{y^{(0)}(i)}}{\left(\frac{(1-e^{a})^{-1}}{y^{(0)}(1)}\right)^2+\sum_{i=2}^{n}\left(\frac{e^{-a(i-1)}}{y^{(0)}(i)}\right)^2}e^{-at_k}\tag{49}$$

In addition, in a control system using grey predictor, the predictor step affects directly on the system working performance. In case of using a fixed step size, the predictor with a small step size speeds up the system response but causes large overshoot or oscillation. Otherwise, the predictor with a large step reduces the overshoot but increases the rising time. To enlarge the efficiency of using this prediction for control design, in this study, this step is self-adjusted accordingly to the control error. In addition, an evaluating factor is used to define the current predictor step size based on the last step and the currently intended step to evaluate whether the predicted value is suitable for the control target or not. The grey predictor step size p in Eq. (37) at a time sequence $(t+1)^{th}$ is, therefore, modified as follows:

$$p(t+1)=\gamma\ (t+1)p\ (t)+(1-\gamma\ (t+1))p_{fuzzy}(t+1)\tag{50}$$

Here, two fuzzy sets, named fuzzy prediction step (FPS) and fuzzy evaluation factor (FEF), are used to in turn generate the factors in Eq. (49): FPS p and fuzzy evaluating factor $\gamma(t)$. For these fuzzy designs, triangle-type membership function is used as presented as (see Ref. 35 for more detail):

$$f_j(x_i)=\begin{cases}1+\dfrac{(x_i-a_{ij})}{b_{ji}^{-}} & if\ \ (-b_{ij}^{-})\le(x_i-a_{ij})\le 0\\ 1-\dfrac{(x_i-a_{ij})}{b_{ij}^{+}} & if\ \ 0\le(x_i-a_{ij})\le(b_{ij}^{+})\\ 0 & otherwise\\ i=1,2;\ j=1,2,...,N.\end{cases}\tag{51}$$

3.4.4 The second grey prediction model GM_2 (1,1)

The purpose of using the GM_2 (1,1) model is to predict the effect of the noises and disturbances to the system at the coming step in order to create the corresponding compensated control signal. Therefore, the process to set up the GM_2 (1,1) model is similar as that of the GM_1 (1,1) model shown in the previous section, except the input raw data sequence. Here, the data sequence is the system response, $e_{ff}^{(0)}$, caused by the noises and disturbances as:

$$\begin{cases}e_{ff}^{(0)}=\left\{e_{ff}^{(0)}(1),e_{ff}^{(0)}(2),...,e_{ff}^{(0)}(m)\right\};\ m\ge 4\\ e_{ff}^{(0)}(k)=y^{(0)}(k)-\hat{y}^{(0)}(k);\ k=1,2,...,m\end{cases}\tag{52}$$

By using the second grey model, GM_2 (1,1), the estimated system response affected by the perturbations at the coming step of time, $(n+1)^{th}$, is given

$$\hat{e}_{ff}^{(0)}(n+1)=\left(e_{ff}^{(1)}(1)-\frac{b_{ff}}{a_{ff}}\right)e^{-a_{ff}(n)}+\frac{b_{ff}}{a_{ff}}\tag{53}$$

Finally, the compensated control signal with respect to the estimated perturbation affecting to the system at the coming step of time, $(n+1)^{th}$, is obtained:

$$\begin{aligned}&\Delta u(t+1)\ \equiv\Delta\hat{y}(t+1)=k_{GP}\times e_{ff}^{(0)}(n+1);\\&\left(k_{GP}\ \text{is a gain factor}\right)\end{aligned}\tag{54}$$

4. Experimental Results

The ability of the proposed control strategy applied to the force and position control of the EHDS is verified in this section by a series of experiments in the comparison with the other semi-parallel controllers. Here, the control system is built in MATLAB/Simulink with with Real-time Windows Target Toolbox of Matlab. To make the perturbed movement, a large noise source containing the band-limited white noises and the sine wave noise is generated real time from the PC during the system operation as given:

$$Dis(t)=A\sin(\omega t)+Rnd(t)\tag{55}$$

where, A and ω are the amplitude and frequency of the sinusoidal noise; $Rnd(t)$ is the white noise signal with power density p_{wn}. These

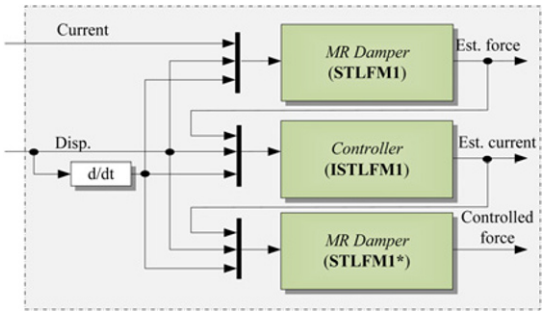

Fig. 9 Simulation program for testing the ISTLFM controller

parameters, A, ω and p_{wn}, were changed randomly within ranges [0, 1], [0.2p, p], and [0.001, 0.02], respectively, to generate the random disturbances. The noise signal generated in Eq. (55) is continuously added to the feedback displacement signal from the control system output with a chosen gain to make a challenge for the position control problem.

Firstly, as the descriptions for the proposed force-sensorless control method, the designed ISTLFM1 controller was firstly examined by simulations before its application to the real-time semi-parallel control. Therefore, a simulating scheme for the ISTLFM1 controller validation was built as in Fig. 9. As seen in this figure, the validating force control system contains three main blocks. The two blocks labeled as 'STLFM1' and 'STLFM1*' are similar and represent for the optimized STLFM model. These blocks then function as the actual MR fluid dampers. The remained block is the ISTLFM1 controller which was designed from section 3.1.

The goal of the validation process is using the ISTLFM1 model to control the second damper model, STLFM1*, to create the damping force to follow the reference force given from the first damper model, STLFM1. Therefore, a displacement/velocity signal was generated and input into both the two damper models and the force controller. A current command signal was applied to the first damper model, STLFM1. The output of this model, called the first simulated damping force, was used as a reference force signal for the damping system based on the second damper model, STLFM1*, and the ISTLFM1 controller. Hence, corresponding to a force command sent from the STLFM1, the ISTLFM1 generated a simulated current command to control the damper model STLFM1*. This simulated current was then fed into the STLFM1* together with the applied displacement/velocity to produce the second simulated damping force. As a result, the validation process carried out the comparison between the reference current command and simulated current command obtained from the ISTLFM1, and the comparison between the first and second simulated damping forces. Consequently, the validating simulation results for the force-sensorless damping control system based on the STLFM and ISTLFM1 corresponding to the sinusoidal signal is shown in Fig. 10. The figures show the system using the ISTLFM1 controller with the virtual sensor STLFM tracked the desired damping force well.

Secondly, experiments on the EHDS were carried out to prove the effectiveness of designed SPC controller with position control problem. In this case, the motion generator will be controlled by the SPC controller to track the desired target, while the force generator works as a 'disturbance generator' to generate the disturbed load of damping

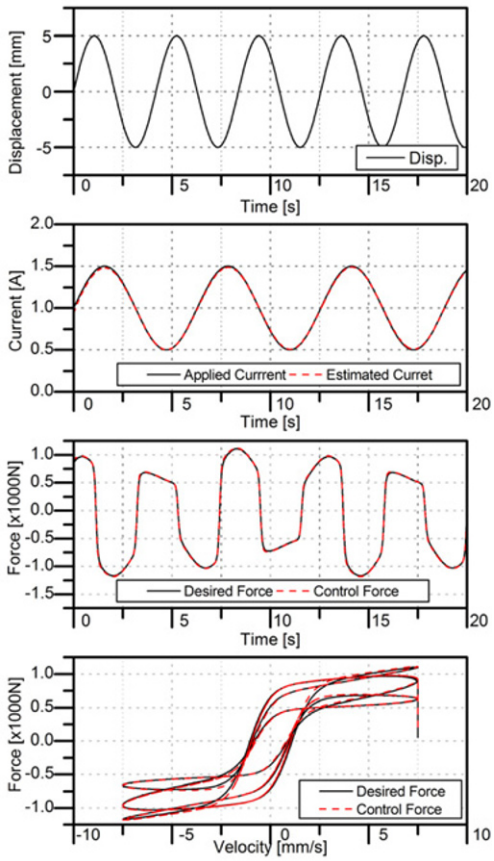

Fig. 10 Force-sensorless control simulation performances using proposed models corresponding to a sinusoidal excitation

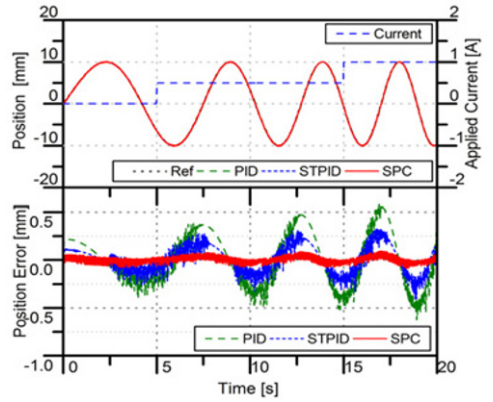

Fig. 11 Position control performances using SPC controller corresponding to a chirp excitation

system. The experiments for the EHDS were done in case the working condition contains the large disturbances. Fig. 11 displays the displacement responses of the EHDS corresponding to a chirp excitation (10 mm, [0.1-0.5] Hz) using the conventional PID controller (kP = 0.724, kI = 0.213, kD = 0.031), self-tuning PID controller[42] and the proposed SPC controller. The results show that the EHDS using the traditional PID controller and self-tuning PID controller are unable to obtain the acceptable displacement control performances when the

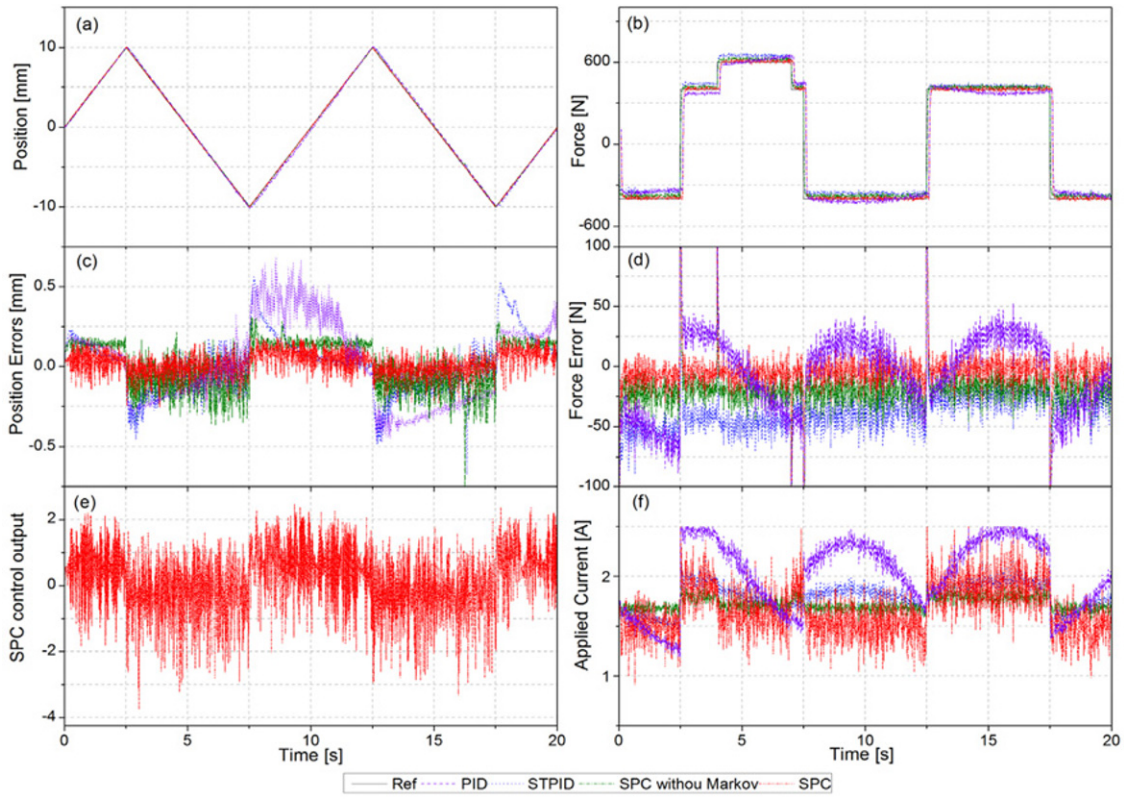

Fig. 12 Semi-parallel position/force-sensorless control performance corresponding to a saw-tooth excitation of position and multi-step excitation of force using different controllers

system operates in the working environment including the large disturbances. On the contrary, the SPC controller still has enough ability to control the EHDS system with high accuracy even in the large varying environment perturbation.

Finally, the proposed semi-parallel control technique was applied to EHDS to perform the control target. The desired force and position was given to verify the effectiveness of the proposed controller as in (56). Figs. 12 and 13 represent the comparison between the designed semi-parallel control strategy using conventional PID controller, STPID controller, SPC controller without Markov chain in grey predictor system and the proposed SPC controller.

$$ref = \begin{bmatrix} x_r \\ f_r \begin{cases} \le 0, & if \quad \dot{x}_r \ge 0 \\ > 0, & if \quad \dot{x}_r < 0 \end{cases} \end{bmatrix} \tag{56}$$

The position tracking results and the force tracking performances are shown in the sub-plots (a) and (b) of these figures, respectively. Besides, the system actuations are analyzed in the subplots (c) to (f).

As the results shown in the sub-plots (a) and (b) of Figs. 12 and 13 with the dash-dot-red lines, it is clearly that the semi-parallel position/force-sensorless control using the SPC controller always achieved the better control performances. The system responses in this case were faster, more accurate and stable than those of the other controllers. These results prove the effectiveness of the proposed control method in which the nonlinear PID controller and SGMP are implemented. The capability of the SGMP in forecasting the position is depicted in Fig. 14 and analyzed in Fig. 15 using three evaluation criteria: root mean square error (RMSE), average relative error (ARE) and coefficient of determination (R2) which are defined as (57), (58) and (59), respectively.

It is clear that the high prediction accuracy could be achieved by using the SGMP. Based on the SGMP information, the control gains were online optimized in advanced with respect to the estimated control error using the robust tuning mechanism. Furthermore, the bad effects of noises and disturbances were remarkably eliminated by the compensating control action produced by the SGMP. As a result, the precise tracking performances were enhanced by the proposed SPC controller.

$$\mathrm{RMSE} = \sqrt{\frac{1}{n}\sum_{k=1}^{n}\left(y^{(0)}(k) - \hat{y}^{(0)}(k)\right)^2} \tag{57}$$

$$\mathrm{ARE} = \frac{1}{n}\sum_{k=1}^{n}\left(\frac{\left|y^{(0)}(k) - \hat{y}^{(0)}(k)\right|}{y^{(0)}(k)} \times 100\right), [\%] \tag{58}$$

$$\mathrm{R2} = 1 - \frac{\sum_{k=1}^{n}\left(y^{(0)}(k) - \hat{y}^{(0)}(k)\right)^2}{\sum_{k=1}^{n}\left(y^{(0)}(k) - \bar{y}\right)^2} \tag{59}$$

5. Conclusion

In this paper, an advanced semi-parallel control algorithm for application to simultaneous position/force-sensorless control of EHA

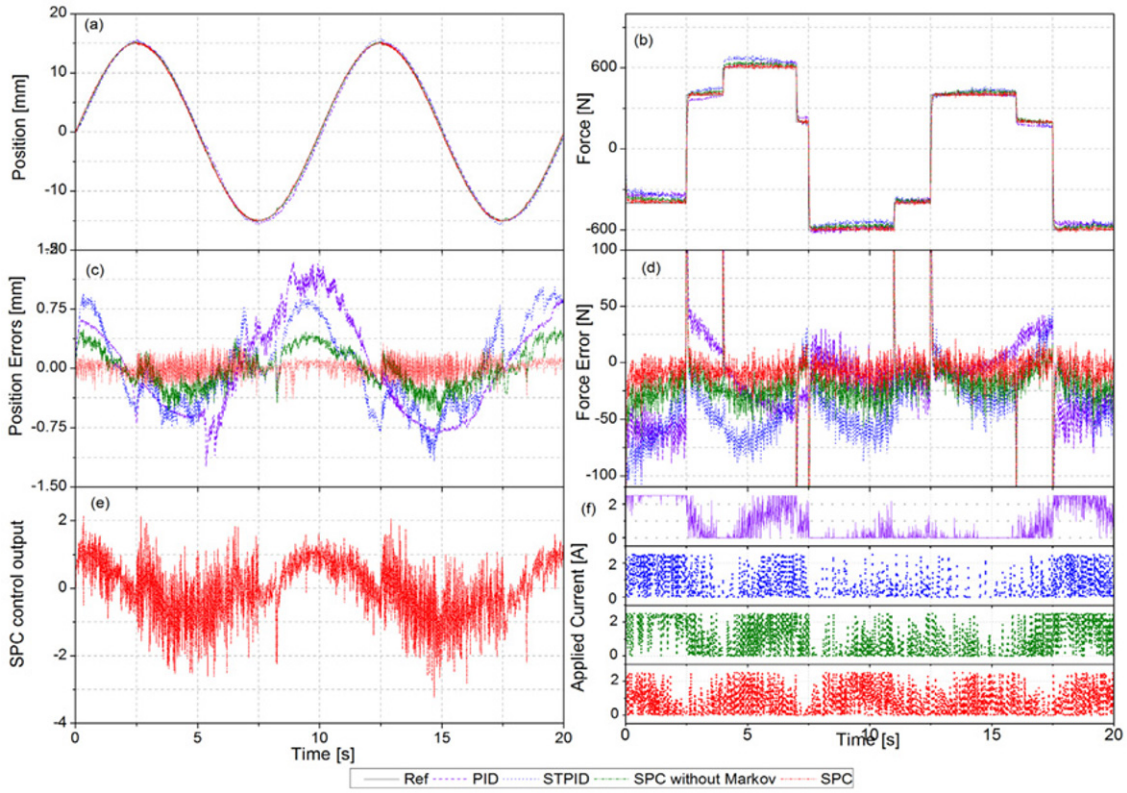

Fig. 13 Semi-parallel position/force-sensorless control performance corresponding to a sinusoidal excitation of position and multi-step excitation of force using different controllers

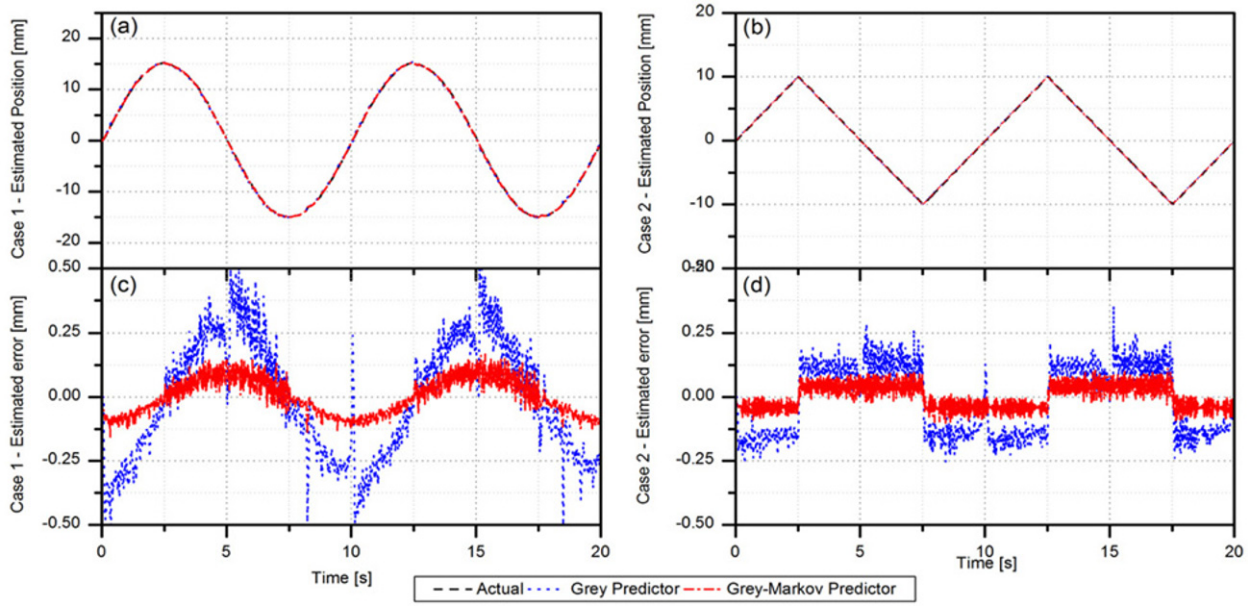

Fig. 14 Comparative results of position prediction in two cases using Grey predictor and Grey-Markov predictor

system using MR fluid damper is proposed. The control strategy is a combination of the smart predictive control, and MR fluid damper identification techniques using a STLF approach. The SPC control approach is constructed from the nonlinear PID controller, and the SGMP. Meanwhile, an observation of the previous system output values is constituted into the SGMP to estimate the output in the near future with the dynamic prediction step size which is fed back to the main controller to obtain the control input. Moreover, an additive correction to the control signal is introduced to another inverse model, to estimate the additive control signal of the MR fluid damper based on

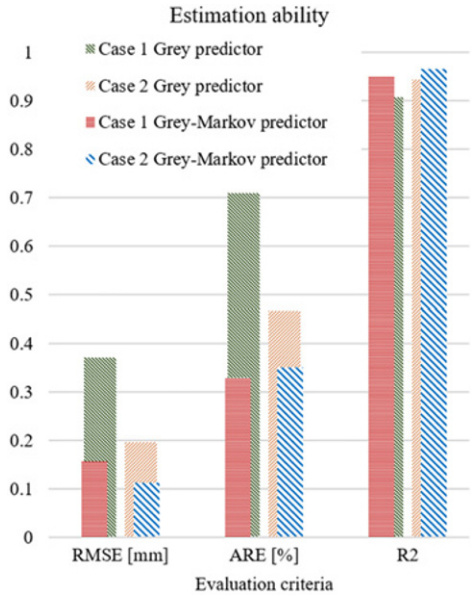

Fig. 15 SGMP estimation ability comparison

the predicted displacement error information given by the SGMP. This additive signal is then sent to the force control system to balance the position and force control performance as well as to compensate for the influences of noises and disturbances and, subsequently, performs the closed-loop control system.

To validate the designed control method, the EHDS test rig using the EHA and MR fluid damper was implemented to investigate the proposed semi-parallel control performance. The comparative study with the other controllers was then conducted for the full evaluation. The comparison results by mean of real-time experiments shown that the best control performance could be always achieved by the proposed controller. This method promises a feasible solution for semi-parallel position/force-sensorless control of EHDS in industrial applications.

ACKNOWLEDGEMENT

This work was supported by the Technology Innovation Program (10043810, Development of a 20-40kW smart hybrid power pack for industry based on intelligent control) funded By the Ministry of Trade, Industry & Energy (MI, Korea) and by the Ministry of Trade, Industry & Energy (MOTIE, Korea) under Industrial Technology Innovation Program (No.10067184).

REFERENCES

1. Zhang, Q. W., Han, L. L., Xu, F., and Jia, K., "Research on Velocity Servo-based Hybrid Position/Force Control Scheme for a Grinding Robot," Advanced Materials Research, Vols. 490-495, pp. 589-593, 2012.
2. Alfayad, S., Ouezdou, F. B., Namoun, F., and Gheng, G., "High Performance Integrated Electro-Hydraulic Actuator for Robotics-Part I: Principle, Prototype Design and First Experiments," Sensors and Actuators A: Physical, Vol. 169, No. 1, pp. 115-123, 2011.
3. Alfayad, S., Ouezdou, F. B., Namoun, F., and Gheng, G., "High Performance Integrated Electro-Hydraulic Actuator for Robotics. Part Ii: Theoretical Modelling, Simulation, Control & Comparison with Real Measurements," Sensors and Actuators A: Physical, Vol. 169, No. 1, pp. 124-132, 2011.
4. Niksefat, N. and Sepehri, N., "Design and Experimental Evaluation of a Robust Force Controller for an Electro-Hydraulic Actuator via Quantitative Feedback Theory," Control Engineering Practice, Vol. 8, No. 12, pp. 1335-1345, 2000.
5. Lizalde, C., Loukianov, A., and Sanchez, E., "Force Tracking Neural Control for an Electro-Hydraulic Actuator via Second Order Sliding Mode," Proc. of the 2005 IEEE International Symposium on Mediterrean Conference on Control and Automation Intelligent Control, pp. 292-297, 2005.
6. Yao J., Jiao, Z. and Yao, B., "Robust Control for Static Loading of Electro-Hydraulic Load Simulator with Friction Compensation," Chinese Journal of Aeronautics, Vol. 25, No. 6, pp. 954-962, 2012.
7. Chen, Y. N., Lee, B. C., and Tseng, C. H. A., "A Variable-Structure Controller Design for an Electrohydraulic Force Control Servo System," The Journal of the Chinese Society of Mechanical Engineers, Vol. 11, No. 6, pp. 520-526, 1990.
8. Conrad, F. and Jensen, C. J. D., "Design of Hydraulic Force Control Systems with State Estimate Feedback," Proc. of 10th Triennial IFAC World Congress, pp. 307-312, 1987.
9. Tsao, T.-C. and Tomizuka, M., "Robust Adaptive and Repetitive Digital Tracking Control and Application to a Hydraulic Servo for Noncircular Machining," Journal of Dynamic Systems, Measurement, and Control, Vol. 116, No. 1, pp. 24-32, 1994.
10. Vossoughi, G. and Donath, M., "Dynamic Feedback Linearization for Electrohydraulically Actuated Control Systems," Journal of Dynamic Systems, Measurement, and Control, Vol. 117, No. 4, pp. 468-477, 1995.
11. Liem, D. T., Truong, D. Q., Park, H. G., and Ahn, K. K., "A Feedforward Neural Network Fuzzy Grey Predictor-based Controller for Force Control of an Electro-Hydraulic Actuator," Int. J. Precis. Eng. Manuf., Vol. 17, No. 3, pp. 309-321, 2016.
12. Bitaraf, M. and Hurlebaus, S., "Semi-Active Adaptive Control of Seismically Excited 20-Story Nonlinear Building," Engineering Structures, Vol. 56, pp. 2107-2118, 2013.
13. Weber, F., "Semi-Active Vibration Absorber based on Real-Time Controlled MR Damper," Mechanical Systems and Signal Processing, Vol. 46, No. 2, pp. 272-288, 2014.
14. Lee, H.-G., Sung, K.-G., Choi, S.-B., Park, M.-K., and Park, M.-K., "Performance Evaluation of a Quarter-Vehicle MR Suspension System with Different Tire Pressure," Int. J. Precis. Eng. Manuf., Vol. 12, No. 2, pp. 203-210, 2011.
15. Kim, H.-J., "Passive and Semi-Active Shock Reduction for

Prototype HSRMD Avoiding Human Damage," Int. J. Precis. Eng. Manuf., Vol. 12, No. 2, pp. 219-225, 2011.

16. Ahmed, G. M. S., Reddy, P. R., and Seetharamaiah, N., "Experimental Investigation of Magneto Rheological Damping Effect on Surface Roughness of Work Piece during End Milling Process," Int. J. Precis. Eng. Manuf., Vol. 13, No. 6, pp. 835-844, 2012.
17. Yi, K. and Song, B., "A New Adaptive Sky-Hook Control of Vehicle Semi-Active Suspensions," Proceedings of the Institution of Mechanical Engineers, part D: Journal of Automobile Engineering, Vol. 213, No. 3, pp. 293-303, 1999.
18. Mizuno, T., Kobori, T., Hirai, J.-i., Matsunaga, Y., and Niwa, N., "Development of Adjustable Hydraulic Dampers for Seismic Response Control of Large Structure," Proc. of ASME PVP Conference, pp. 163-170, 1992.
19. Kwok, N. M., Ha, Q. P., Nguyen, T. H., Li, J., and Samali, B., "A Novel Hysteretic Model for Magnetorheological Fluid Dampers and Parameter Identification using Particle Swarm Optimization," Sensors and Actuators A: Physical, Vol. 132, No. 2, pp. 441-451, 2006.
20. Vadtala, I. H., Soni, D. P., and Panchal, D. G., "Semi-Active Control of a Benchmark Building using Neuro-Inverse Dynamics of MR Damper," Procedia Engineering, Vol. 51, pp. 45-54, 2013.
21. Wang, D. H. and Liao, W. H., "Modeling and Control of Magnetorheological Fluid Dampers using Neural Networks," Smart Materials and Structures, Vol. 14, No. 1, pp. 111-126, 2004.
22. Peng, G. R., Li, W. H., Du, H., Deng, H. X., and Alici, G., "Modelling and Identifying the Parameters of a Magneto-Rheological Damper with a Force-Lag Phenomenon," Applied Mathematical Modelling, Vol. 38, No. 15, pp. 3763-3773, 2014.
23. Schurter, K. C. and Roschke, P. N., "Fuzzy Modeling of a Magnetorheological Damper using ANFIS," Proc. of the 9th IEEE International Conference on Fuzzy Systems, pp. 122-127, 2000.
24. Wang, D.-H. and Liao, W.-H., "Neural Network Modeling and Controllers for Magnetorheological Fluid Dampers," Proc. of the 10th IEEE International Conference on Fuzzy Systems, pp. 1323-1326, 2001.
25. Kwok, N. M., Ha, Q. P., Nguyen, M. T., Li, J., and Samali, B., "Bouc-Wen Model Parameter Identification for a MR Fluid Damper using Computationally Efficient GA," ISA Transactions, Vol. 46, No. 2, pp. 167-179, 2007.
26. Liem, D. T., Truong, D. Q., and Ahn, K. K., "Hysteresis Modeling of Magneto-Rheological Damper using Self-Tuning Lyapunov-based Fuzzy Approach," Int. J. Precis. Eng. Manuf., Vol. 16, No. 1, pp. 31-41, 2015.
27. Ahn, K. K., Chau, N. H. T., and Truong, D. Q., "Robust Force Control of a Hybrid Actuator using Quantitative Feedback Theory," Journal of Mechanical Science and Technology, Vol. 21, No. 12, pp. 2048-2058, 2007.
28. Brosilow, C. and Joseph, B., "Techniques of Model-based Control," Prentice Hall Professional, pp. 221–237, 2002.
29. Haugen, F., "Exercises to Basic Dynamics and Control," TechTeach, 2010.
30. Julong, D., "Introduction to Grey System Theory," The Journal of Grey System, Vol. 1, No. 1, pp. 1-24, 1989.
31. Truong, D. Q. and Ahn, K. K., "Wave Prediction based on a Modified Grey Model MGM (1, 1) for Real-Time Control of Wave Energy Converters in Irregular Waves," Renewable Energy, Vol. 43, pp. 242-255, 2012.
32. Lian, R.-J., "Enhanced Adaptive Grey-Prediction Self-Organizing Fuzzy Sliding-Mode Controller for Robotic Systems," Information Sciences, Vol. 236, pp. 186-204, 2013.
33. Barrios, J. A., Torres-Alvarado, M., and Cavazos, A., "Neural, Fuzzy and Grey-Box Modelling for Entry Temperature Prediction in a Hot Strip Mill," Expert Systems with Applications, Vol. 39, No. 3, pp. 3374-3384, 2012.
34. Guo, H., Xiao, X., and Forrest, J., "A Research on a Comprehensive Adaptive Grey Prediction Model CAGM (1, N)," Applied Mathematics and Computation, Vol. 225, pp. 216-227, 2013.
35. Liem, D. T., Truong, D. Q., and Ahn, K. K., "A Torque Estimator Using Online Tuning Grey Fuzzy PID for Applications to Torque-Sensorless Control of DC Motors," Mechatronics, Vol. 26, pp. 45-63, 2015.
36. Lin, J. and Lian, R.-J., "Design of a Grey-Prediction Self-Organizing Fuzzy Controller for Active Suspension Systems," Applied Soft Computing, Vol. 13, No. 10, pp. 4162-4173, 2013.
37. Zeng, B., Meng, W., and Tong, M., "A Self-Adaptive Intelligence Grey Predictive Model with Alterable Structure and Its Application," Engineering Applications of Artificial Intelligence, Vol. 50, pp. 236-244, 2016.
38. Liu, C., Shu, T., Chen, S., Wang, S., Lai, K. K., and Gan, L., "An Improved Grey Neural Network Model for Predicting Transportation Disruptions," Expert Systems with Applications, Vol. 45, pp. 331-340, 2016.
39. Damásio, B. and Nicolau, J., "Combining a Regression Model with a Multivariate Markov Chain in a Forecasting Problem," Statistics & Probability Letters, Vol. 90, pp. 108-113, 2014.
40. Carpinone, A., Giorgio, M., Langella, R., and Testa, A., "Markov Chain Modeling for Very-Short-Term Wind Power Forecasting," Electric Power Systems Research, Vol. 122, pp. 152-158, 2015.
41. Jiang, P. and Liu, X., "Hidden Markov Model for Municipal Waste Generation Forecasting Under Uncertainties," European Journal of Operational Research, Vol. 250, No. 2, pp. 639-651, 2016.
42. Ahn, K., Truong, D., Thanh, T., and Lee, B., "Online Self-Tuning Fuzzy Proportional-Integral-Derivative Control for Hydraulic Load Simulator," Proceedings of the Institution of Mechanical Engineers, Part I: Journal of Systems and Control Engineering, Vol. 222, No. 2, pp. 81-95, 2008.